# Correlation of Canopy Distortion with Asymmetric Loading in Large Diameter Ringsail Parachutes

Samuel A. Janssen[1]
*Jacobs Technology, Houston, TX, 77058*

Eric S. Ray[2]
*National Aeronautics and Space Administration*
*Johnson Space Center, Houston, TX, 77058*

**The second generation of the main parachutes for the Orion Capsule Parachute Assembly System (CPAS) were subjected to multiple flight tests. Three of the tests included were instrumented with the Tension Measuring System (TMS) to record main dispersion bridle loads. While these units were not able to resolve the individual suspension line loads, they were able to record a coarse representation of the asymmetric loading of the main parachutes during inflation. These tests were also equipped with upward looking cameras mounted on the test vehicles to collect detailed imagery of main deployment and inflation. When analyzed independently, both data sources exhibit similar features. These similarities provide evidence that the suspension line loads and the distortions in the canopy geometry are not independent. This paper will examine both data sources simultaneously to establish a correlation between asymmetric loading at the canopy skirt and the deformations of the canopy. This correlation will be used to build a model which can estimate individual suspension line loads from a measured riser load and detailed imagery.**

## I. Nomenclature

| | | |
|---|---|---|
| $A$ | = | Asymmetric load factor |
| $C_a$ | = | Axial force scaling factor |
| $D_o$ | = | Nominal parachute diameter based on reference area, $\boldsymbol{D_o = \sqrt{4 \cdot S_o/\pi}}$ |
| $F_{bridle}$ | = | Measured tension in a parachute dispersion bridle |
| $F_{riser}$ | = | Measured tension in a parachute riser, parachute axial force |
| $F_{sl_t}$ | = | Tension in parachute suspension line derived from bridle tension measurement |
| $F_{sl_e}$ | = | Estimated tension for individual parachute suspension line |
| $LSF$ | = | Load Scaling Function used to estimate suspension line loads |
| $R$ | = | Radius of radial located on horizontal cross section relative to center of area |
| $\delta$ | = | Radial distortion factor of horizontal cross section |
| S/N | = | Serial Number |

## II. Introduction

The Capsule Parachute Assembly System (CPAS) for the Orion spacecraft utilizes three pilot deployed 116 ft $D_o$ ringsail main parachutes. Following an extensive test program and four design generations, the CPAS system was qualified and accepted for use at the CPAS System Acceptance Review (SAR) in September of 2019. The second

[1] Analysis Engineer, Aerosciences and Flight Mechanics, 2224 Bay Area Blvd, Houston TX, non-member
[2] Analysis Engineer, Aeroscience Branch, NASA Johnson Space Center/EG3, AIAA Senior Member.

generation of mains utilized eight dispersion bridles which collected ten suspension lines each to convey their load into the riser. These bridles were removed from later generations, but while in use, presented the ability to instrument clusters of suspension lines.[1]

Three Cluster Development Tests (CDT) were executed with TMS units equipped. Two of the tests, CDT-2-1 and CDT-2-2, were demonstrations of two main clusters and CDT-2-3 demonstration of a three main cluster. The TMS units usefully collected data and indicated bridle level asymmetry factors as high as 1.9.[1]

The mechanics that produce the asymmetric loading phenomenon are complex and believed to be the result of a coupling between canopy structure and aerodynamic loads.[2] This coupling produces a circular relationship for the root cause. While the root cause may be indeterminate, the coupling, results in the canopy the geometry being a driving contributor to the canopy loading during inflation.

A recent re-examination of CPAS TMS data has resulted in a refinement of the determined asymmetry factors. A novel approach was developed to resolve the measured suspension dispersion bridle loads into individual suspension line loads.[3] This approach has produced data that allows for further investigation into the coupling of canopy geometry to asymmetric loading.

## III.Methodology

Tests of the CPAS system recorded both asymmetric loads and videos of inflating main canopies. These two data sources can be resolved into snapshots of key events to begin the process of correlation. When the loads data are reduced to singular time step, a convenient method of visualizing data is through the use of a polar plot of the asymmetric loading factors.[2] Originally proposed by Schmidt et al, this allows for the plotting of a nondimensional factor in a format consistent with the radial locations where the measurements were taken during a test. This commonality in format also allows for an initial qualitative comparison between measurements and canopy distortion.

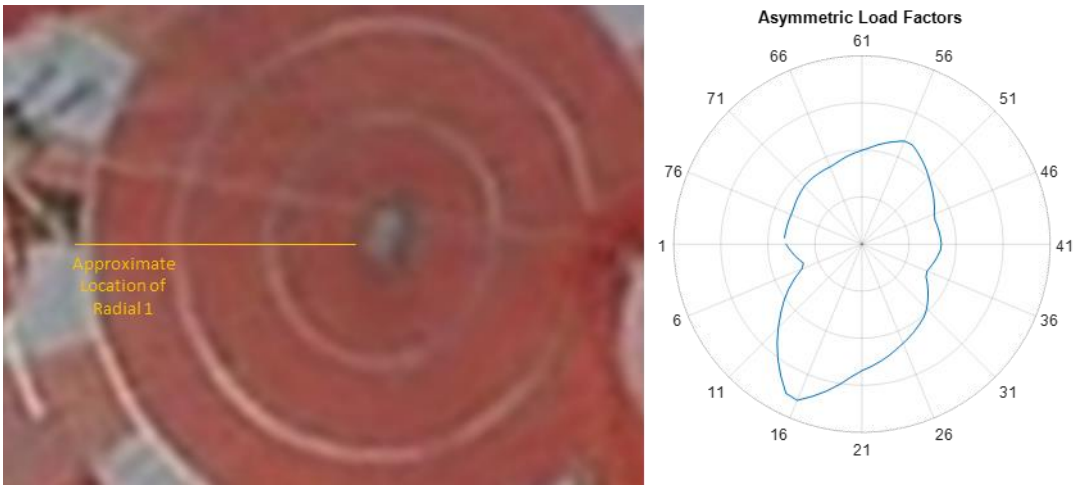


**Figure 1. CDT 2-1 Crown distortion (left) and asymmetric load factors (right) at full open peak load.**

In Figure 1, when a polar plot of the asymmetric loading factors is oriented alongside of the observed canopy distortion, it can be seen that both metrics tend to be elliptical. Close examination of the imagery also indicates that the concavity in the load factor trace is related to the curvature of the crown. Between radials 31 – 41 in Figure 1, the curvature of the crown is relatively flat. At the vent, the curvature may even be concave. This region corresponds to a concave region on the load factor trace. Using these observations, a mapping of suspension line loading to canopy deformations can be derived.

A derived mapping of canopy loading to canopy deformation is desired to be a function of the tension in a parachute riser and a measure of canopy distortion. The CPAS test project was able to collect substantial amounts of riser data and imagery but was only able to collect limited asymmetric loading data. If a function can be derived which utilizes riser tension measurements and imagery to estimate asymmetric load factors, it could be applied to tests other than the CDT tests with instrumented bridles and greatly expand the understanding of CPAS main parachute performance. Therefore, it is also desirable for a non-dimensional factor for the deformation of the canopy to be defined. This will allow for a model which has a tensile load as both input and output. With these features in mind, a formulation can begin to be derived.

If the crown of the canopy is assumed to be planar where the distortion is observed, the distortion factor can be reduced to two dimensions. If we extract a planar cross section located along the outside edge of each ring, a polygon can be created using the approximate locations of the parachute's radials. The defined polygon can then be used to calculate a center of area which in turn can be used to calculate a radius for each radial. Equation 1 defines a simple ratio of the individual radii to the mean results in a non-dimensional radial distortion factor (δ).

$$\delta = \frac{\mathrm{R}}{mean(\mathrm{R})} \tag{1}$$

Unfortunately, CDT test imagery is not able to resolve the exact radial locations in the canopy. Therefore, a method of approximation must be utilized. The small gaps between rings provides the ability to determine the outline of a given ring and canopy markings allow the approximate location of the first radial to be determined. If it is assumed that the radial spacing is uniform about the ring, locations can be estimated around the circumference starting at a known location. Using the approximated radial locations, the distortion factor for each radial can be calculated.

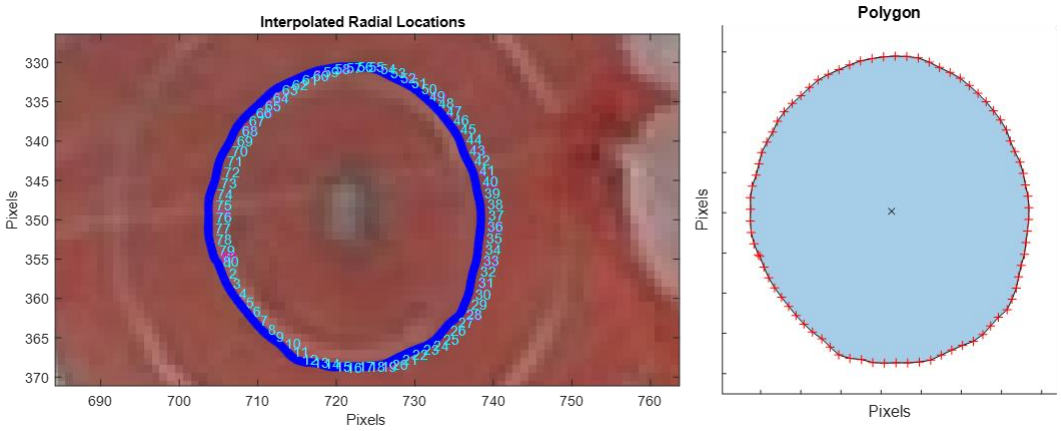


**Figure 2. CDT 2-1 S/N 2 Ring 1 resultant radial positions and polygon.**

The distortion factor can then be compared against the asymmetric load factor for each radial location. A simple co-plot of the asymmetric load factor and the distortion factor yields a distinct correlation. Using this relation, a Load Scaling Function (LSF) can be defined by the best fit of data.

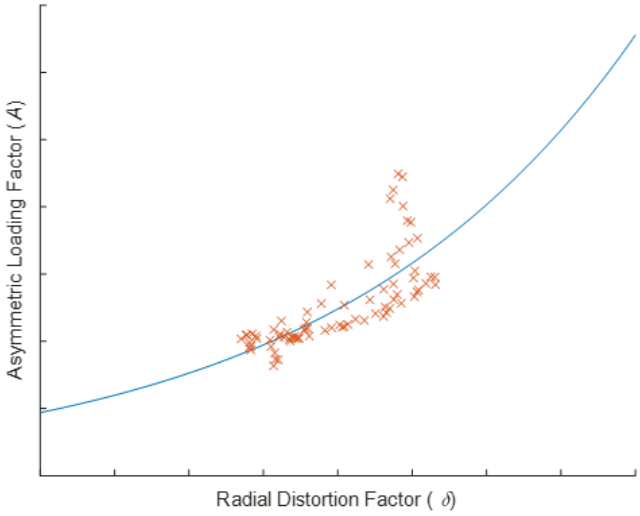


**Figure 3. CDT 2-1 S/N 2 Ring 1 asymmetric load factor and radial distortion correlation.**

Since the LSF is a function of two non-dimensional parameters, a suspension line load can be calculated simply as the product of the LSF and the total axial load of the parachute in question (Eq. 2). Since the data do not have a perfect

correlation, a final axial scaling factor ($C_a$), must be introduced to ensure the sum of the axial force of suspension lines does not violate the total axial force of the parachute. When all information is then combined, a relatively simple formulation for estimating the tension in suspension lines is produced as shown in Eq. 3.

$$F_{sl_e} = \mathrm{LSF}(\delta) * F_{riser} \tag{2}$$

$$F_{riser} = \sum_{j=1}^{j=80} C_a * \left(F_{sl_e}\right)_j \tag{3}$$

## IV. Test Data and Correlation

### A. CDT 2-1

CDT 2-1 was intended to test a two main cluster with two reefed stages per canopy. An unplanned skipped second stage occurred on the S/N 2 main. The skipped second stage resulted in a substantial suppression of inflation to full open for the S/N 1 main. This suppression resulted in a loss of useful full open asymmetry data on the S/N 1 main. Fortunately, both asymmetry data and imagery were captured for the S/N 2 main at the moment of full open peak load.

The position of the canopy and the geometry of the skirt for S/N 2 allowed for the observation of the first three rings in the crown of the canopy and the position of the skirt. For the first and second rings from the apex, the outer edge of the rings could be directly observed. For the third ring and skirt however, short regions were blocked from view by the skirt and harness lines respectively. In these regions, the edges were visually interpolated based on the observed curvature to obtain an estimate of the edge of the ring and of the skirt. With the perimeters of the rings and skirt defined, the positions of the radials could be calculated.

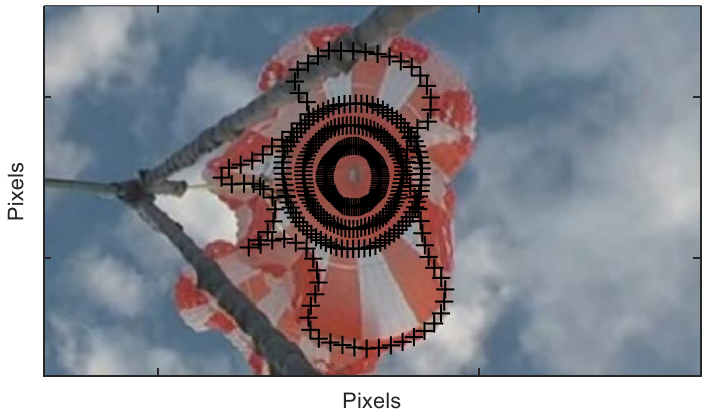


**Figure 4. CDT 2-1 S/N 2 radial locations at full open peak load.**

Using the extracted locations, four radial distortion factor datasets are created corresponding to their respective ring or skirt. The datasets are separated as each ring exhibits similar, but distinct trends which can be seen in Figure 5. An exponential function is shown fitted to each dataset. For main S/N 2, strong correlation can be observed in rings one through three. The skirt visually has a correlation, but high asymmetric loading factors at moderate distortion factors leads to weak overall correlation.

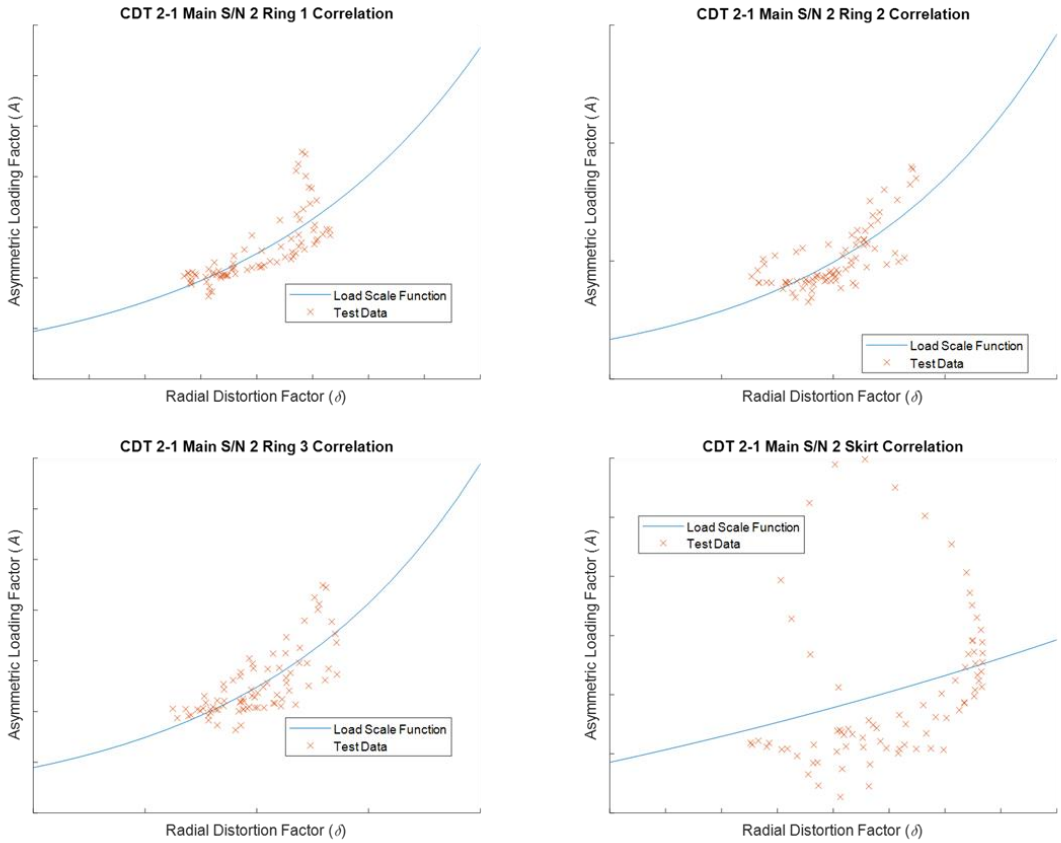


**Figure 5. CDT 2-1 S/N 2 radial distortion factor correlation to asymmetric loading factor.**

## B. CDT 2-2

CDT 2-2 was a test of a two main cluster with nominal reefing schedules. Imagery and asymmetric loading data were collected for both canopies at during full open peak load. While imagery was collected for both mains, equivalent analysis could not be completed for both mains. The resolution of the available cameras only allowed for the extraction of radial locations at the skirt of the S/N 4 main as imagery is not sufficient to resolve the edges of the rings in the crown of the S/N 4 main. The extracted locations for the S/N 4 main can be overserved in Figure 6.

Using the extracted locations, the distortion factors for the skirt were calculated and compared to the asymmetric loading factors. This correlation can be seen in Figure 7 where the dataset has been fitted with an exponential function. The plotted datasets show a strong correlation between the asymmetric loading factors and the radial distortion factors of the skirt. The correlation for the skirt on CDT 2-2 S/N 2 is substantially stronger than the correlation for the skirt on the CDT 2-1 S/N 2 main.

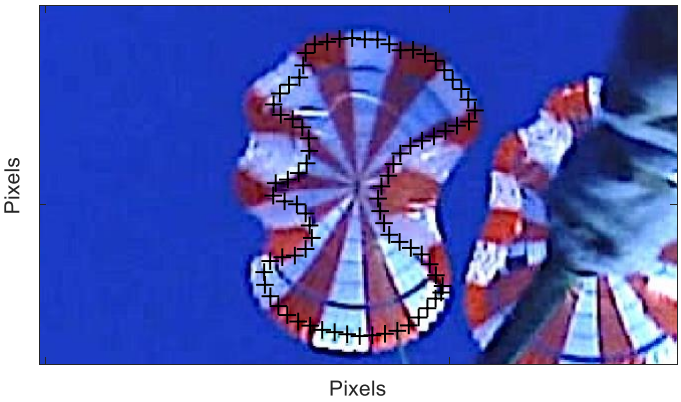


**Figure 6. CDT 2-2 S/N 4 radial locations at full open peak load.**

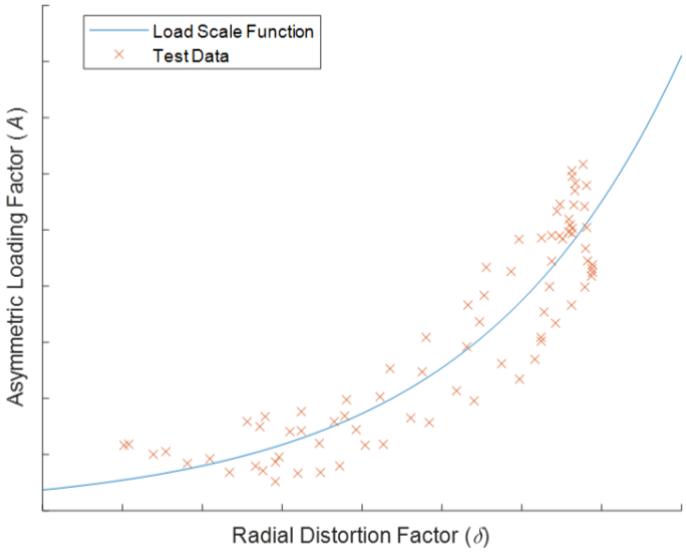


**Figure 7. CDT 2-2 S/N 4 radial locations at full open peak load.**

While imagery limited the analysis of the S/N 4 main, the imagery allowed for the extraction radial positions along the edges of the first three rings at the crown as well as the skirt for the S/N 5 main. A few regions of the skirt were blocked from view by a suspension sling, but these regions were small enough that the skirt shape can reasonably visually interpolated. The extracted radial positions can be observed in Figure 8.

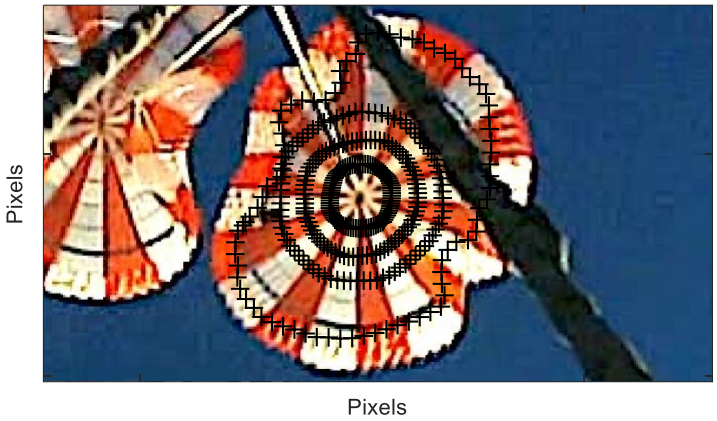


**Figure 8. CDT 2-2 S/N 5 radial locations at full open peak load.**

Using these four datasets, asymmetric loading and radial distortion can be correlated. This correlation is presented in Figure 9 where they are fit with exponential functions. With four planar cross sections, the CDT 2-2 S/N 5 main exhibits correlation similar to the CDT 2-1 S/N 2 main. In Figure 9, it can be seen that the Ring 1, Ring 3, and Skirt datasets show strong correlation between the radial distortion factors and the asymmetric loading factors. The skirt's correlation supports the strong correlation seen in the CDT 2-2 S/N 4 main skirt. Correlation can also be observed in Ring 2, but it is not as strong as the other planar cross sections. The correlation in the CDT 2-2 S/N 5 Ring 2 does not appear to be as strong as that for the CDT 2-1 S/N 2 Ring 2.

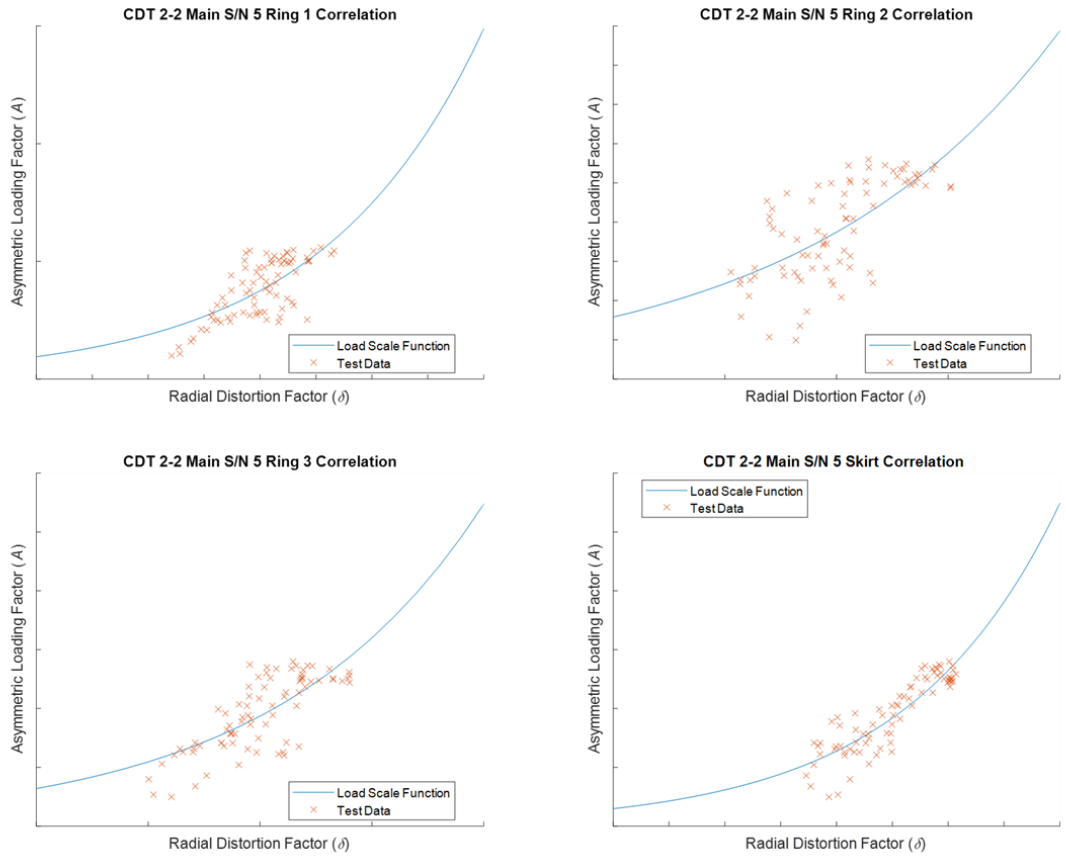


**Figure 9. CDT 2-2 S/N 5 radial distortion factor correlation to asymmetric loading factor.**

## C. CDT 2-3

CDT 2-3 was a test of a three main cluster with nominal reefing schedules. Unfortunately, limited hardware prevented the instrumenting of all three mains for collection of asymmetric loading data and asymmetric loading data was only collected for two canopies.

Imagery for both the S/N 3 main and the S/N 4 main had limited resolution. The locations of radials at the skirt could be extracted, but radial locations along rings in the crown could not be determined accurately. The extracted locations at their respective peak loads can be seen in Figure 10.

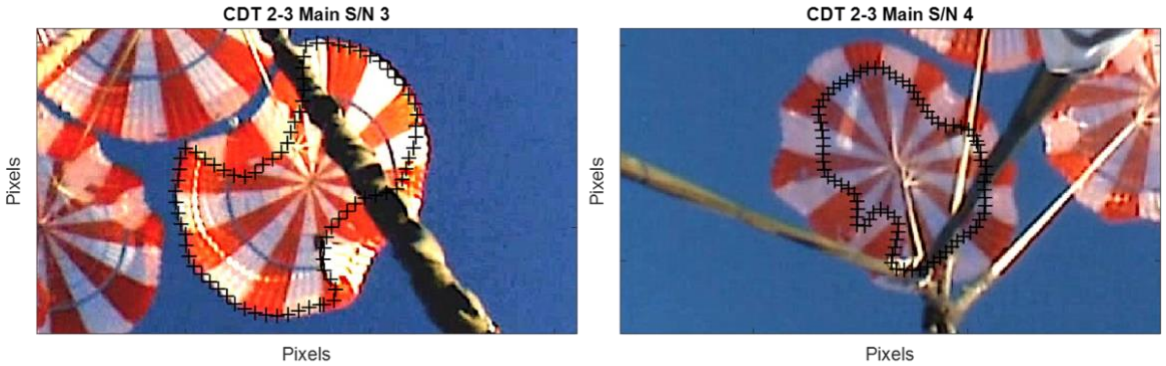


**Figure 10. CDT 2-3 S/N 3 and S/N4 radial locations at full open peak load.**

The correlation of the extracted locations is presented in Figure 11 where the data are shown fit with an exponential function. Data for both canopies show a strong correlation between radial distortion factors for their skirts and their

asymmetric loading factors. The observed correlation corroborates the correlation observed for the skirts of the CDT 2-2 mains.

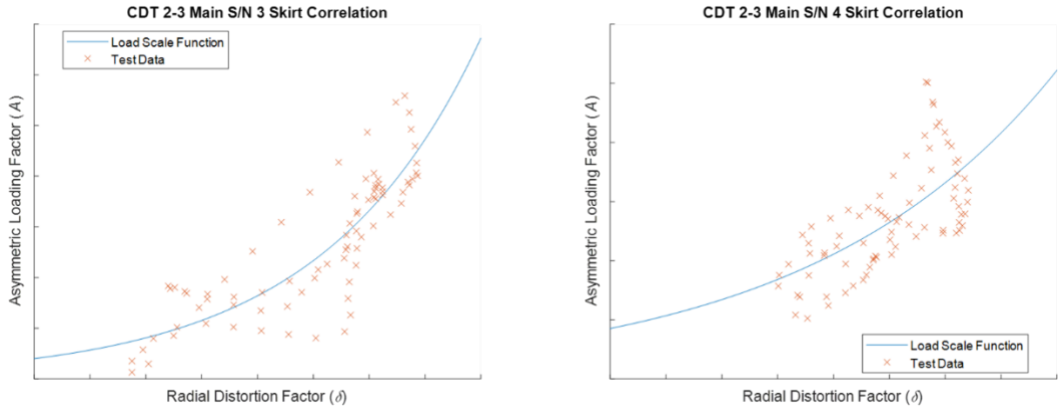


**Figure 11. CDT 2-3 S/N 3 & S/N 4 radial distortion factor correlation to asymmetric loading factor.**

## D. Cumulative Data

A review of data for each planar cross section of the canopies with data shows a distinct correlation between canopy distortions and asymmetric suspension line loading. Aside from this conclusion, each individual data set is of limited use. For the observations to have use as an analysis tool, the datasets for each respective ring and skirt must be combined and interrogated. The combined datasets are plotted in Figure 12 fitted with exponential functions.

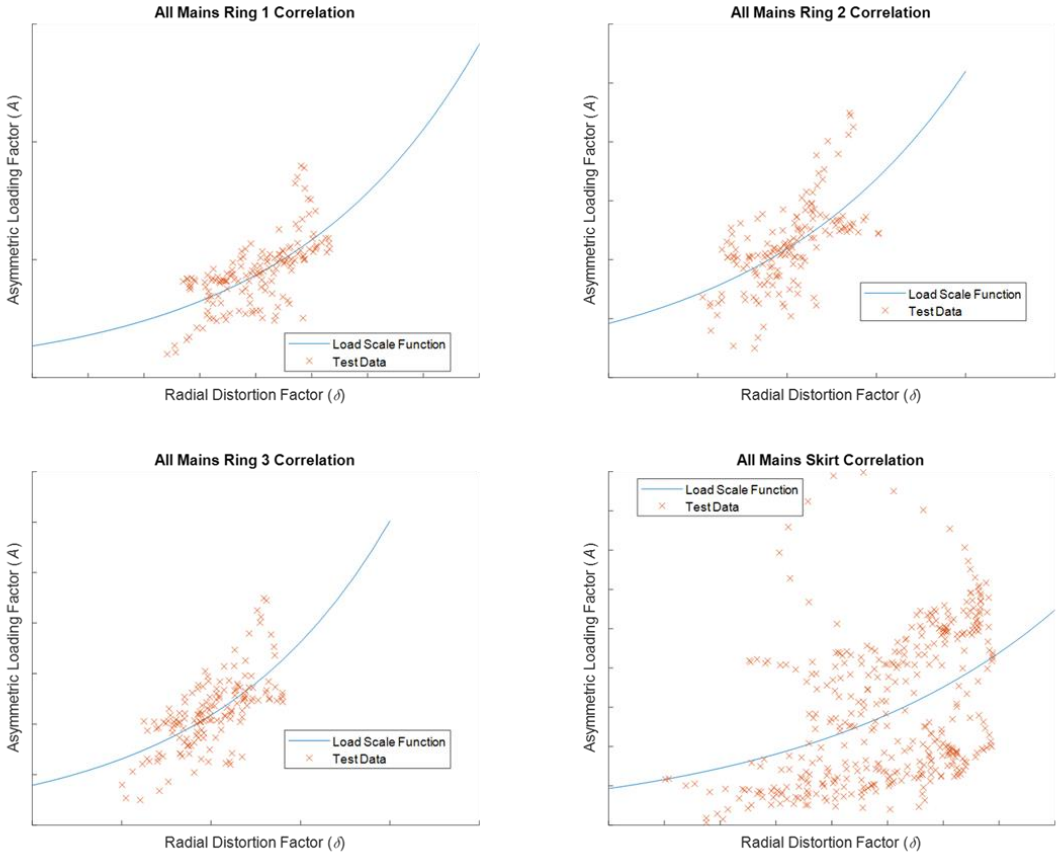


**Figure 12. Combined radial distortion factor correlation to asymmetric loading factor.**

The cumulative data shown Figure 12 indicate that the correlations noted in individual datasets is not unique to a specific canopy within a test. The combined datasets all exhibit a strong correlation between radial distortion factors and asymmetric loading factors. Visually, it appears that that the first three rings in the crown of a canopy exhibit a stronger correlation than the skirt.

In Table 1, the accuracy of three fitting functions is presented. While all three functions provide similar adjusted R-squared values, an exponential fit is believed to provide the best fit. A quadratic fit tends to be adequate within the domain of recorded data but is inadequate outside the test data domain. Below the domain of test data, quadratic fits tend to increase such that a very low distortion factor would estimate a high asymmetric load factor which is nonsensical. A fit using a power function preforms nearly identically to an exponential fit but was unable to consistently fit the test data with a consistent concavity.

**Table 1. Adjusted R-Squared Values for Cumulative Data Fit**

| Planar Cross Section | Quadratic | Power | Exponential |
|---|---|---|---|
| **Ring 1** | 0.4355 | 0.4394 | 0.4396 |
| **Ring 2** | 0.3727 | 0.3751 | 0.3742 |
| **Ring 3** | 0.4492 | 0.4425 | 0.4409 |
| **Skirt** | 0.1738 | 0.1740 | 0.1766 |

The adjusted R-squared values of the applied exponential fits shown in Table 1 corroborate the visual observation that the canopy crowns exhibit stronger correlation than the skirt. The source of this difference is unknown but there are a few plausible explanations. It could be the result of sample size with only having two datasets for the rings while having four data sets for the skirt. It could also be indicative of the complex coupling the structural grid with the asymmetric loading of canopies. The nature of the canopy construction allows the skirt to experience substantially larger deformations than the crown. Additionally, when video is viewed, the skirt deformations are substantially more dynamic. The combination of dynamic and large deformations of the skirt supports a conclusion that the discrepancy is not the result of sample size differences.

The quality of the applied fits can also be inspected via a review of their respective residuals. Histograms of the residuals are shown in Figure 13. A review of the residuals shows that rings one through three would likely be best fit with a normal distribution. The skirt, however, appears to show that a log normal may be required to adequately capture the tail of the distribution. It is likely that this difference is related to the noted differences between correlation within the crown and at the skirt.

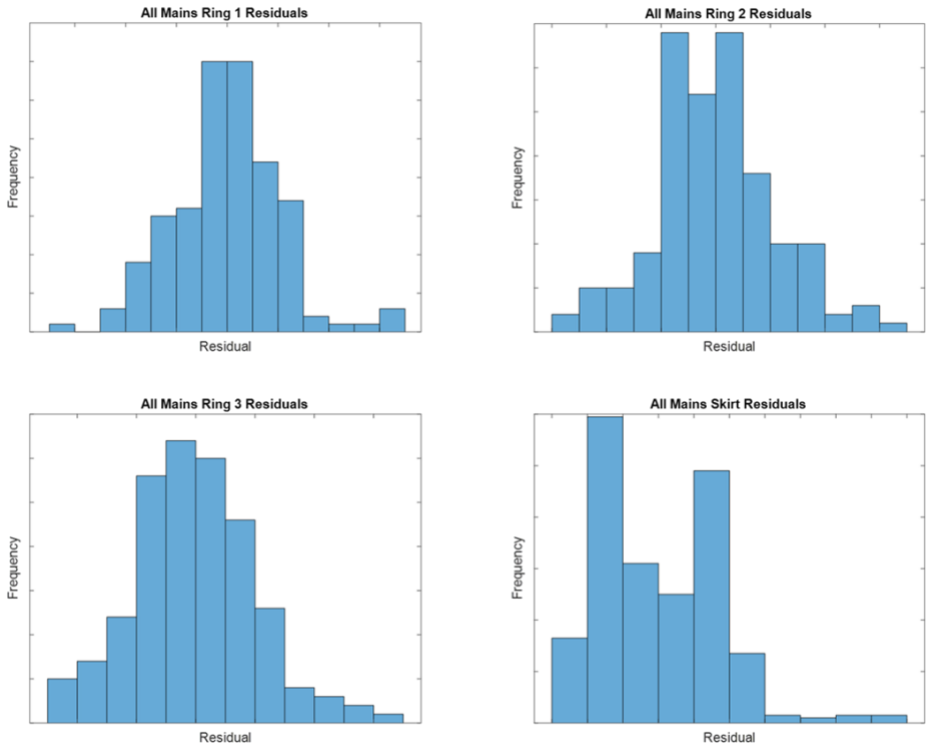


**Figure 13. Residuals of fitted cumulative datasets.**

## V. Estimated Loads and Accuracies

### A. Estimated Load Traces

Using the Load Scaling Functions defined by the fit of the cumulative datasets, it is possible to estimate the suspension line loads for the tested canopies. By applying the Load Scaling Functions shown in Figure 12 and discussed in Table 1 and Figure 13, suspension line loads can be estimated using Equations 1 and 2. The results of these load predictions can be evaluated for accuracy by using three different criteria. The first method is a qualitative assessment based on the visual comparison between the estimated suspension line load traces and measured suspension line loads in a polar coordinate frame. The second method reviews the accuracy of the predicted suspension line load for the suspension line with the peak load. The third method reviews the accuracy of the peak predicted suspension line load.

The estimated loads for the CDT 2-1 S/N 3 main are shown below in Figure 14. In Figure 14, it can be seen that the load traces estimated using the first three rings in the crown closely resemble the load traces created using test data. The estimated load trace created using the skirts radial distortion loosely resembles the test data. Overall, the estimated loads closely resemble the measured test data visually.

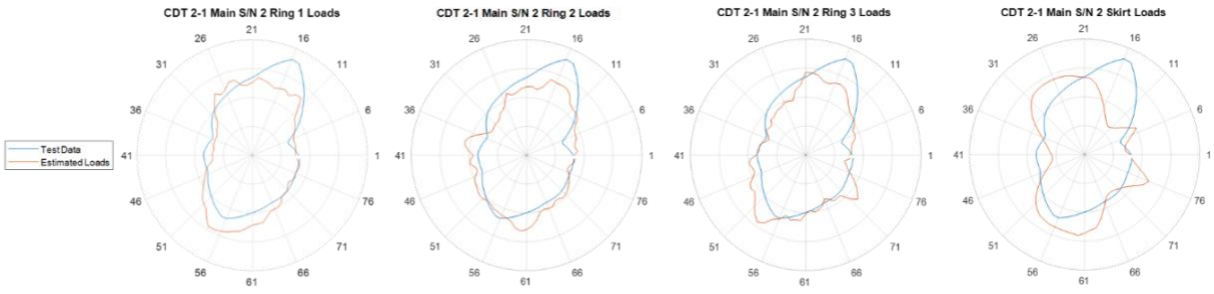


**Figure 14. CDT 2-1 S/N 2 estimated suspension line loads.**

The estimated loads for the CDT 2-2 S/N 4 main are shown to the right in Figure 15. Comparing the two load traces, the estimated load trace closely resembles the trace from test data. While the peaks are not captured, there are several unique features that are captured very well. Both the traces from test data and the predicted traces exhibit a local peak near suspension line 51 and the local minima near suspension line 31 and suspension line 71.

For the S/N 5 main on CDT 2-2, it can be seen in Figure 16 that the estimated traces closely resemble the traces from test data for both the first three rings in the crown as well as skirt. The estimates using the crown do exhibit a few sporadic peaks near suspension line 30 and 70 that are local peaks rather than the local minimums of the test data. The source of these peaks is suspected to be a product of imagery resolution. It is believed that an increased resolution in imagery would result in improved radial distortion factors that would smooth out the curves.

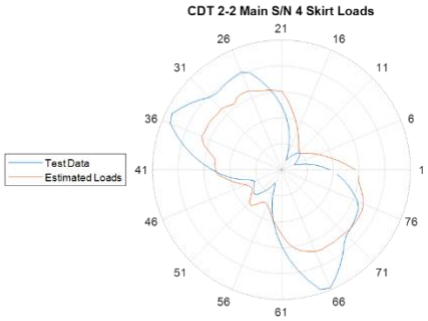


**Figure 15. CDT 2-2 S/N 4 estimated suspension line loads.**

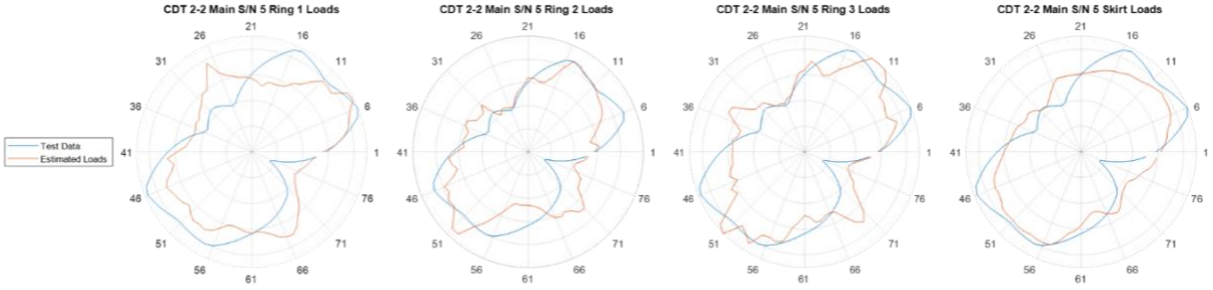


**Figure 16. CDT 2-2 S/N 5 estimated suspension line loads.**

The estimated loads using the skirt for CDT 2-3 resemble the traces from test data, but the S/N 3 main exhibits a better match than the S/N 4 main. In Figure 17, it can be observed the trace for the S/N 3 main closely resembles the trace for the majority of the trace and only experiences a large divergence near suspension line 36. For the S/N 4 main, approximately half of the predicted trace reasonably resembles the trace from test data.

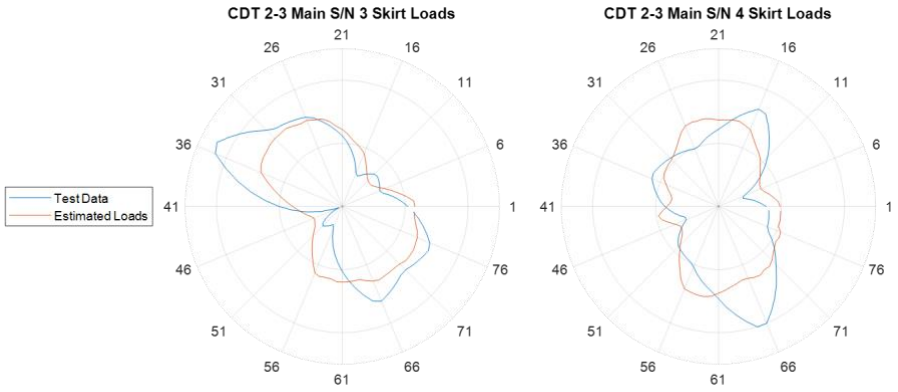


**Figure 17. CDT 2-3 S/N 3 & 4 estimated suspension line loads.**

### B. Estimated Peak Load Errors

When reviewing the predicted peak loads, there are two methods that can be used. The first method is a comparison between the predicted load for the suspension line with the observed peak load. This criterion allows for the determination of the percent error for consistent suspension line peak loads. The second method is to compare the predicted peak load with the observed peak loads. Using this method, the percent error for inconsistent suspension

line peak loads can be determined. The errors for these two methods can be seen in Table 2 and Table 3. The average percent error for each planar cross section using both methods can be observed Table 4.

**Table 2. Percent Error for Consistent Suspension Line Peak Load Prediction**

| Main | Ring 1 | Ring 2 | Ring 3 | Skirt | Average |
|---|---|---|---|---|---|
| **CDT 2-1 S/N 2** | -30.5% | -24.7% | -25.4% | -50.8% | -32.9% |
| **CDT 2-2 S/N 4** | | | | -30.8% | -30.8% |
| **CDT 2-2 S/N 5** | -7.2% | -24.3% | -22.4% | -15.5% | -17.4% |
| **CDT 2-3 S/N 3** | | | | -35.2% | -35.2% |
| **CDT 2-3 S/N 4** | | | | -39.1% | -39.1% |

**Table 3. Percent Error for Inconsistent Suspension Line Peak Load Prediction**

| Main | Ring 1 | Ring 2 | Ring 3 | Skirt | Average |
|---|---|---|---|---|---|
| **CDT 2-1 S/N 2** | -19.4% | -23.3% | -20.4% | -21.6% | -21.2% |
| **CDT 2-2 S/N 4** | | | | -29.0% | -29.0% |
| **CDT 2-2 S/N 5** | -0.5% | 4.3% | 0.4% | -13.2% | -2.3% |
| **CDT 2-3 S/N 3** | | | | -31.8% | -31.8% |
| **CDT 2-3 S/N 4** | | | | -28.0% | -28.0% |

**Table 4. Percent Error for Cumulative Peak Load Predictions**

| Planar Cross Section | Consistent Peak Load | Inconsistent Peak Load |
|---|---|---|
| **Ring 1** | -18.8% | -10.0% |
| **Ring 2** | -24.5% | -9.5% |
| **Ring 3** | -23.9% | -10.0% |
| **Skirt** | -34.3% | -24.7% |
| **Average** | -25.4% | -13.5% |

Two conclusions can be drawn from the tables. First, the inconsistent peak loads predictions are roughly twice as accurate as the consistent peak load predictions. Second, regardless of method used, the peak loads are always underpredicted.

The technique used for approximation and the structural grid of the canopies likely combine to produce the observed discrepancy. The structural grid of the canopy provides complex interconnected load paths for the applied asymmetric loads. The complex load paths and the rigidity inherent to the structural grid likely smooths radial distortions. Effectively, the canopy cannot distort at the same rate that the loads may rise. Additionally, the method of interpolation used to define the edges of the planar cross sections results in a smoothing to the radial distortion factors. The use of a nominal fit applies a further smoothing to the data. The discrepancy between the two peak load predictions is therefore one that can be expected.

While it would be desirable for the two peak load predictions to converge, for practical use, it is not required. Due to the symmetric nature of most canopies, the specific radial with the peak load is not typically required for engineering calculations. As long as the estimated peak suspension line loads is accurate, the exact suspension with the load is not necessary.

The observation that peak loads are consistently underestimated is also one which is expected. The application of only a nominally fit Load Scaling Function means suspension line loads will never be overestimated. Observed peak loads are above average while the predictions are always on average. This underprediction is an issue that would need solved prior to the use of this method for engineering purposes.

Two methods exist that could potentially solve the issue of underpredicted loads. Nominally, a bias could be applied to offset the predicted loads. With sufficient test data, an average offset could be determined and applied to the peak predicted loads. A second approach would be to review the probability of peak loads rather than strictly the nominal loads. With sufficient test data, usable prediction intervals for the Load Scaling Function could be determined. These prediction intervals could be used to estimate the maximum, minimum, and the most likely experienced peak load.

Unfortunately, CPAS was only able to collect limited data during the projects drop test campaign that likely prevents a reasonable application of either of these methods.

## VI. **Conclusion**

A review of CPAS TMS data which was recently resolved from bridle load tension measurements into suspension line tension measurements has been reviewed in conjunction with imagery of canopy radial distortion.[3] This review was able to define radial distortion factors and a Load Scaling Function which can be used to estimate suspension line loads from riser tension measurements and imagery. This correlation definitively shows that asymmetric suspension line loads are transferred from the skirt to the crown and vent of a canopy in large diameter ringsail parachutes. With sufficient data, it is believed the presented method of analysis could be calibrated to a specific canopy and used to analyze asymmetric loads factors for large diameter ringsail parachute when only riser tension and imagery is available.

## Acknowledgements

The authors would like to thank Aaron B. Comis and John J. Rangel formerly of the NASA Commercial Crew Parachutes Team for their contribution to asymmetric loading analysis. Jared Daum of the Johnson Space Center Engineering division contributed key insight into the mechanics of parachute construction and component loading which informed development of this analysis technique.

## References

[1] Morris, A. L., Olson, L., and Taylor, T., "Load Asymmetry Observed During Orion Main Parachute Inflation," *21st AIAA Aerodynamics Decelerator Systems Technology Conference*, Dublin, Ireland, May 2011, AIAA paper 2011-2611.
[2] Schmidt, J. R., McFadden, P. G., and Pritchett, V. E., "Parachute Asymmetry in Ares Development Tests," *21st AIAA Aerodynamics Decelerator Systems Technology Conference*, Dublin, Ireland, May 2011, AIAA paper 2011-2575.
[3] Ray, E. S, "Orion Main Parachute Asymmetry Testing Revisited," *26th AIAA Aerodynamics Decelerator Systems Technology Conference*, Toulouse, France, May 2022 (not yet published)